A transmission/escape probabilities model for neutral particle transport in the outer regions of a diverted tokamak

1994 Nucl. Fusion 34 1385

(http://iopscience.iop.org/0029-5515/34/10/I07)

A TRANSMISSION/ESCAPE PROBABILITIES MODEL FOR NEUTRAL PARTICLE TRANSPORT IN THE OUTER REGIONS OF A DIVERTED TOKAMAK

W.M. STACEY, Jr., J. MANDREKAS
Fusion Research Center,
Nuclear Engineering Programme,
Georgia Institute of Technology,
Atlanta, Georgia,
United States of America

ABSTRACT. A new computational model for neutral particle transport in the outer regions of a diverted tokamak plasma chamber is presented. The model is based on the calculation of transmission and escape probabilities using first-flight integral transport theory and the balancing of fluxes across the surfaces bounding the various regions. Both long and short mean free path regions can be handled. The complex geometry of the outer regions of a diverted tokamak can be represented accurately and economically using precomputed probabilities which depend only on the mean free path of the region. Benchmark comparisons with Monte Carlo illustrate that quite accurate results may be expected with the method.

1. INTRODUCTION

The transport of neutral atoms and molecules of fuel and impurity species in the 'outer regions' — the edge plasma, the scrape-off layer (SOL), the divertor channels and the plasma chamber and divertor plenums — of a diverted tokamak is a computational problem the practical significance of which is being increasingly recognized. There are indications that conditions in the plasma edge may control the energy confinement of the bulk plasma, and such conditions in turn may be influenced by the neutral population in the outer regions. More directly, the interaction among neutrals and plasma ions and electrons in the outer regions is being relied on to 'radiatively cool' the latter and thereby reduce the heat load on the divertor collection plate, which is presently predicted to be excessive in next-generation devices such as ITER.

The importance of neutral particle transport in the outer regions of plasmas has long been recognized by specialists, and a variety of computational models have been used, as reviewed in Ref. [1]. Thus, it is incumbent upon anyone who would introduce a new computational model, which is the purpose of this paper, to comment upon the existing models and to indicate why a new model is needed, which we do in Appendix A.

The method which is proposed in this paper utilizes the integral transport method to do what it does best, calculate the uncollided neutral flux that is transmitted from one surface to another. The secondary source in the intervening region is then found by subtraction, and the collided neutral flux through surrounding surfaces is then calculated from an escape probability formulated from integral transport theory. The concept is to break the outer regions of a diverted tokamak plasma up into a relatively small number of complex geometrical regions and to do a balance on the fluxes crossing the surfaces bounding these regions, using surface-to-surface transmission probabilities calculated with integral transport theory and region-to-surface escape probabilities based on the repeated application of first-flight transport calculations of escape probabilities. The treatment of the transmitted fluxes is similar to that in the collision probability methods of neutron transport theory, but the calculation of intraregion transport via multiple flight escape probabilities to enable the use of large regions is novel. With a few plausible assumptions, the transmission and escape probabilities depend only upon the geometry and the mean free path of the region, so that complex geometries can be represented in precomputed transmission and escape probabilities which can be stored as a function of the mean free path and looked up at run time, thereby eliminating the computational penalty of complex geometry. With another plausible assumption, the region-to-surface escape probabilities can be written as simple expressions involving the surface area, volume and mean free path of the region. The most limiting assumption on the method is that of uniform properties (or at least known property variation) within a region, which places a lower limit on the number of regions required for a given accuracy.

This paper is organized as follows. Definitions of quantities involved in neutral transport are given in

Section 2, and a representative geometrical model for the outer regions of a diverted tokamak is given in Section 3. The fluxes across surfaces are constructed from uncollided fluxes across other surfaces and from collided fluxes emerging from adjacent regions in Section 4. The solution of the resulting flux equations and the use of that solution in a particle balance are indicated in Section 5. The methodology for calculating transmission probabilities, escape probabilities and the plasma albedo are given in Sections 6–8, respectively. Modifications needed to treat neutral impurity atoms are given in Section 9. Some benchmarking calculations are reported in Section 10. A discussion of assumptions and applications in Section 11 concludes the paper. Explicit expressions for the calculation of transmission probabilities in the model problem geometry are given in Appendices B and C.

2. DEFINITIONS

Γ_{a-b} is the neutral flux from region $a \rightarrow$ region b;

Γ^{b}_{a-c} is the transmission coefficient expressing the probability that neutral particles incident into region b from region a emerge from region b into region c without a collision event;

P_b is the escape probability that a neutral particle 'born' in region b (external source, charge exchange event, electron recombination) or its neutral progeny will escape from region b without being ionized;

Λ_{b-c} is the probability that a neutral particle 'born' in and escaping from region b escapes into adjacent region c;

α_{ab} is the albedo of region b, i.e. the probability that a neutral particle entering region b from region a (or its neutral progeny) re-emerges from region b into region a;

R_{wb} is the reflection coefficient for wall bounding region b, i.e. the probability that a neutral (or charged) particle incident upon the wall is reflected as a neutral particle;

f_{pb} is the fraction of neutrals striking the 'wall' bounding region b that are removed by pumping.

3. MODEL GEOMETRY

A representative geometry of the plasma, SOL, divertor and plenum regions within the plasma and divertor chambers is illustrated for a axisymmetric tokamak with a single null divertor configuration in Fig. 1.

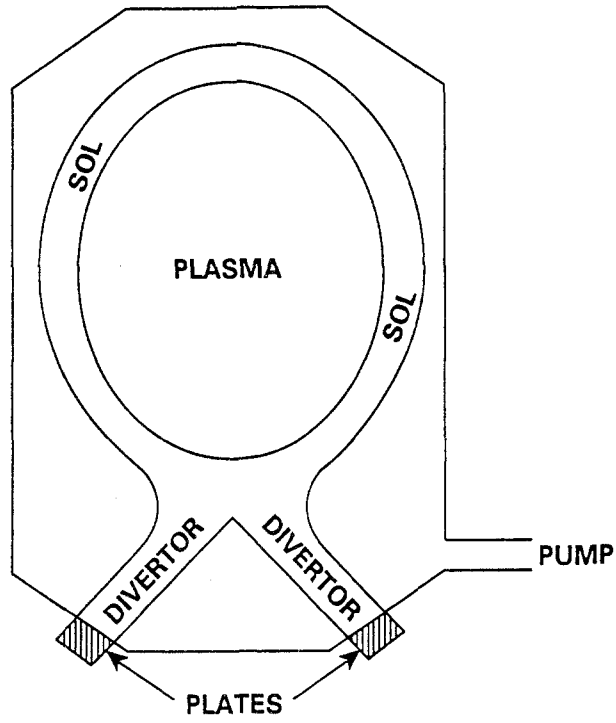

FIG. 1. Single null divertor geometry (not to scale).

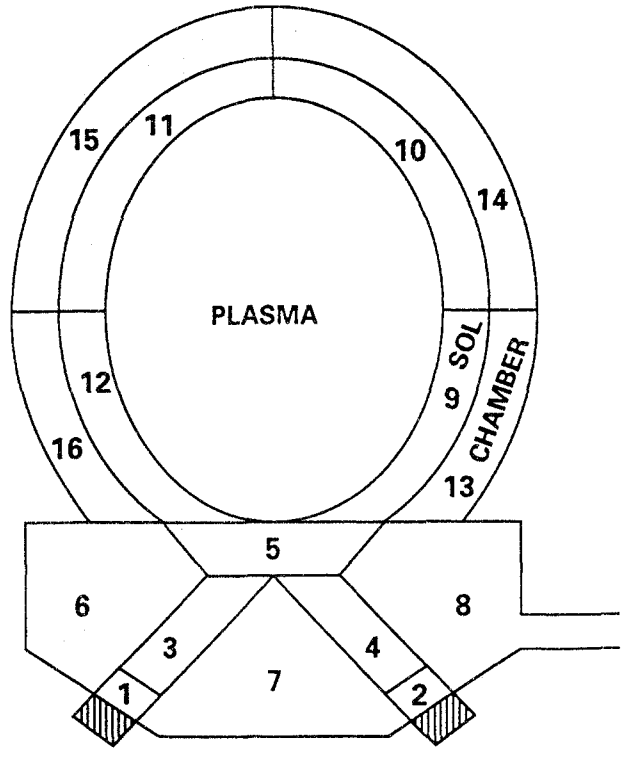

FIG. 2. Geometrical model for outer region neutral calculation.

A simple geometrical model which should represent the actual geometry of Fig. 1 reasonably well is illustrated in Fig. 2. The divertor channel has been divided into a presheath region (1 and 2) which extends a few mean free paths in front of the collector plate, in which intense neutral charged particle interactions take place, and a channel (3 and 4) extending up to the throat (5). All of these regions can be represented by trapezoids. The divertor plenum (6–8) can be represented rather exactly by regions bounded by straight lines. The SOL (9–12) and the plasma chamber (13–16) can be represented approximately by concentric annular segments to allow for treating poloidal asymmetries. The model of Fig. 2 is for the purpose of illustration — the actual geometrical model that would be used in any given calculation would depend on the configuration and the geometrical accuracy required (see Section 10).

4. FLUXES ACROSS SURFACES

The formalism is developed for a neutral hydrogenic atomic species. Modifications to allow treatment of a neutral impurity species are discussed in a subsequent section.

With respect to Fig. 2, the neutral flux emerging from region i into adjacent region j consists of: (1) the sum of the neutral fluxes that entered region i from all adjacent regions times the probabilities that these fluxes emerge without collision into region j

$$\sum_k^i \Gamma_{k-i} T^i_{k-j}$$

where $\sum_k^i$ is the sum over all regions k that are contiguous to region i; plus (2) the sum of all neutral fluxes that entered region i from all adjacent regions and that had a collision in region i

$$\sum_k^i \Gamma_{k-i}\left(1 - \sum_l^i T^i_{k-l}\right)$$

times the probability

$$A^i_{\mathrm{cx}} \equiv \frac{\langle \sigma v\rangle^i_{\mathrm{cx}}}{\langle \sigma v\rangle^i_{\mathrm{cx}} + \langle \sigma v\rangle^i_{\mathrm{ion}}}$$

that the collision was a charge exchange event, times the probability (P_i) that the charge exchange neutral or its progeny eventually escapes from region i, times the probability (Λ_{i-j}) that a neutral particle escaping from region i enters region j; plus (3) the probability that a neutral particle introduced into region i externally (S^i_{ex}) escapes into region j ($P_i\Lambda_{i-j}$)

$$\Gamma_{i-j} = \sum_k^i \Gamma_{k-i}\left[T^i_{k-j} + A^i_{\mathrm{cx}} P_i \Lambda_{i-j}\left(1 - \sum_l^i T^i_{k-l}\right)\right] + S^i_{\mathrm{ex}} P_i \Lambda_{i-j} \quad (1)$$

The flux from a region i in the plasma edge into the adjacent SOL region j is

$$\Gamma_{i-j} = \alpha_{ji}\Gamma_{j-i} \quad (2)$$

Thus it is not necessary to explicitly treat the plasma inside the separatrix in the neutral calculation; rather it is treated as an albedo boundary condition on the inner surface of the SOL.

The neutral flux into region i from a bounding wall region iw is the sum of: (1) the neutral flux from region i to the wall, given by Eq. (1), times the probability ($1 - f_{\mathrm{pi}}$) that this incident flux is not pumped out, times the probability ($R_{\mathrm{w}i}$) that this incident flux is reflected from the wall; plus (2) the ion flux ($\Phi^{iw}_{\mathrm{plate}}$) incident upon the divertor plate — for the presheath regions only — times the reflection coefficient ($R_{\mathrm{w}i}$)

$$\Gamma_{iw-i} = (1 - f_{\mathrm{pi}})R_{\mathrm{w}i}\left\{\sum_k^i \Gamma_{k-i} \times \left[T^i_{k-iw} + A^i_{\mathrm{cx}} P_i \Lambda_{i-iw}\left(1 - \sum_l^i T^i_{k-l}\right)\right] + S^i_{\mathrm{ex}} P_i \Lambda_{i-iw}\right\} + \Phi^{iw}_{\mathrm{plate}} R_{\mathrm{w}i}\delta_{iw,ps} \quad (3)$$

where $\delta = 1$ for the presheath and 0 otherwise.

The transmission probabilities (T^i_{k-j}) involve mean free paths $\lambda = v_0/n\langle\sigma v\rangle$, which should be evaluated using the neutral speed (v^k_0) that is characteristic of the region k from which the neutral has emerged (unless region k is a vacuum region across which the neutral has streamed from region k', in which case ($v^{k'}_0$) should be used) and using $n_i\langle\sigma v\rangle_i$ for the region i.

The reflected neutral flux consists of two components: (1) a fraction χ of neutrals that are reflected with a fraction g of the speed of the incident neutral/ion; and (2) a fraction $1 - \chi$ that thermalize in the wall, are re-emitted as molecules, then dissociate to produce neutrals with the Franck-Condon speed v^{FC}_0

$$\Gamma_{iw-i} = \chi\Gamma^{(g)}_{iw-i} + \Gamma^{(\mathrm{FC})}_{iw-i}(1 - \chi) \quad (4)$$

When calculating the transmission probabilities for these reflected neutrals across the presheath region i, a neutral speed gv^i_0 should be used to evaluate the mean free path for the first component, and a neutral speed v^{FC}_0 should be used to evaluate the mean free path for the second component.

The total ionization rate in region i consists of the ionization of external source neutrals and of neutrals flowing

into region i from adjacent regions, after zero, one, two, three, ... charge exchange events

$$I_i = \left[S^i_{ex} + \sum_k^i \Gamma_{k-i} \left(1 - \sum_l^i T^i_{k-l} \right) \right] \times A^i_{ion} \sum_{n=0}^{\infty} [A^i_{cx}(1 - P_i)]^n = \frac{\left[S^i_{ex} + \sum_k^i \Gamma_{k-i} \left(1 - \sum_l^i T^i_{k-l} \right) \right] A^i_{ion}}{1 - A^i_{cx}(1 - P_i)} \quad (5)$$

where $A^i_{ion} \equiv 1 - A^i_{cx}$.

The presence of impurities is taken into account by defining an effective ionization rate in terms of the plasma ion concentration n_i

$$\langle \sigma v \rangle_{ion} = \langle \sigma v \rangle^i_{ion} + \frac{n_e}{n_i} \langle \sigma v \rangle^e_{ion} + \sum_j \frac{n_{zj}}{n_i} \langle \sigma v \rangle^j_{cx} = \left[\langle \sigma v \rangle^i_{ion} + \left(1 + \frac{\alpha}{Z} \right) \langle \sigma v \rangle^e_{ion} + \frac{\alpha}{Z^2} \sum_j \chi_{zj} \langle \sigma v \rangle^j_{cx} \right] \quad (6)$$

where $\alpha \equiv n_z Z^2 / n_i$ and $\chi_{zj} \equiv n_{zj}/n_z$, with n_z and n_{zj} being the total and jth charge state impurity densities, and $\langle \sigma v \rangle^j_{cx}$ is the charge exchange rate between the neutral hydrogenic species and the jth impurity charge state.

5. SOLUTIONS STEPS

With the assumptions: (1) the plasma properties are uniform (or at least vary in a known way) within a region; (2) the incident neutral flux is isotropic over the inward hemisphere[1]; and (3) the incident neutral flux is uniformly distributed over the surface, the transmission and escape probabilities depend only on the mean free path and geometry of the region. Since the geometry is fixed the transmission and escape probabilities can be precomputed as a function of λ and looked up from a table at run time. Fixed, but non-uniform plasma properties and incident neutral flux distribution, and a prespecified anisotropic angular distribution, could be accommodated within a precomputed table, but it is unlikely that the knowledge of these non-uniformities and anisotropies would be good enough to make this worthwhile.

We obtain $2N$ equations, where N is the number of interfaces, of the type of Eqs (1)–(3). These equations have the general form

$$\mathbf{M\Gamma} = \mathbf{S}_{ex} + \mathbf{\Phi}_{plate} \quad (7)$$

and the general solution

$$\mathbf{\Gamma} = \mathbf{M}^{-1}[\mathbf{S}_{ex} + \mathbf{\Phi}_{plate}] \quad (8)$$

The neutral particle balance equation in each region is

$$\dot{N}_j = S^j_{ex} - \sum_k^j (\Gamma_{j-k} - \Gamma_{k-j}) - N^{ion} \langle \sigma v \rangle^j_{ion} N_j \quad (9)$$

which has the steady state solution

$$N_j = \frac{S^j_{ex} - \sum_k^j (\Gamma_{j-k} - \Gamma_{k-j})}{N^{ion} \langle \sigma v \rangle^j_{ion}} \quad (10)$$

The numerical solution steps are:

(1) Evaluate the transmission and escape probabilities from precomputed tables, using the plasma densities and temperatures to calculate λ;
(2) Solve Eq. (7) for $\mathbf{\Gamma}$ by inverting $\mathbf{M}$;
(3) Use $\mathbf{\Gamma}$ in Eq. (10) to obtain the steady state neutral content or in Eq. (9) to advance the dynamic solution.

6. TRANSMISSION PROBABILITY

With reference to Fig. 3, we are interested in calculating the probability that a flux of neutrals incident upon side 1 of the region emerges uncollided through side 3, for example. We call this probability the transmission probability $T_{1\text{-}3}$.

The uncollided neutral flux is given by

$$\varphi(l) = \varphi(0) e^{-l/\lambda} \quad (11)$$

where

$$\lambda \equiv \frac{v_0}{n_i(\langle \sigma v \rangle_{ion} + \langle \sigma v \rangle_{cx})} \quad (12)$$

and l is the path length from the point of entry into the region.

If the distribution of the incident flux along side 1 is $\Gamma_1(\xi_1, \phi)$, then the transmission probability is

$$T_{1\text{-}3} \equiv \frac{\int_{\xi_1^{min}}^{\xi_1^{max}} d\xi_1 \int_{\phi_{min}(\xi_1)}^{\phi_{max}(\xi_1)} d\phi e^{-l(\phi)/\lambda} \Gamma_1(\xi_1, \phi)}{\int_{\xi_1^{min}}^{\xi_1^{max}} d\xi_1 \int_0^{\pi} d\phi \Gamma_1(\xi_1, \phi)} \quad (13)$$

The angles $\phi_{min}(\xi_1)$ and $\phi_{max}(\xi_1)$ are the minimum and maximum angles ϕ subtended at ξ_1 by the side 3. Now, $l(\phi)$ represents the path length from point ξ_1 on side 1 to point ξ_2 on side 2, as shown in Fig. 3.

[1] This is equivalent to a double-P_0 representation [2].

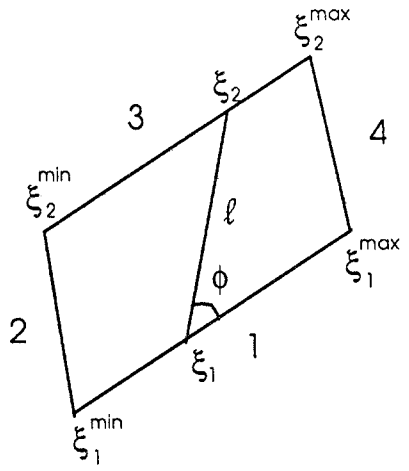

FIG. 3. Surface to surface transmission.

If the incident particle distribution is isotropic over the inward hemisphere, then $\Gamma_1(\xi_1, \phi) \rightarrow \Gamma_1(\xi_1)/\pi$ and Eq. (13) reduces to

$$T_{1\text{-}3} = \frac{\int_{\xi_1^{min}}^{\xi_1^{max}} d\xi_1 \Gamma_1(\xi_1) \frac{1}{\pi} \int_{\phi_{min}(\xi_1)}^{\phi_{max}(\xi_1)} d\phi e^{-l(\phi)/\lambda}}{\int_{\xi_1^{min}}^{\xi_1^{max}} d\xi_1 \Gamma_1(\xi_1)} \quad (14)$$

We further define the local transmission probability that an isotropically distributed neutral incident at point ξ_1 on side 1 emerges uncollided through side 3

$$t_{1\text{-}3}(\xi_1) \equiv \frac{1}{\pi} \int_{\phi_{min}(\xi_1)}^{\phi_{max}(\xi_1)} d\phi e^{-l(\phi)/\lambda} \quad (15)$$

If the incident flux is uniformly distributed along side 1, then the transmission probability reduces to

$$T_{1\text{-}3} = \int_{\xi_1^{min}}^{\xi_1^{max}} d\xi_1 t_{1\text{-}3}(\xi_1)/(\xi_1^{max} - \xi_1^{min}) \quad (16)$$

For a fixed geometry, this quantity depends only on λ. Transmission probabilities are calculated in the appendices for the geometry of Fig. 2.

7. ESCAPE PROBABILITY

We first follow Ref. [3] to develop a first flight escape probability, then use this result to construct a total escape probability.

A neutral particle created by charge exchange at point r_0, with an isotropic distribution, has a probability

$$P_0'(r_0) = \int \frac{e^{-l/\lambda}}{4\pi l^2} (\hat{\Omega} \cdot \hat{n}_s) ds \quad (17)$$

of escaping across the surface bounding the region before having an interaction. With reference to Fig. 4, $\hat{n}_s$ and $\hat{n}_i$ are the outward and inward normal vectors to the surface of the region, $l(r_0, \Omega)$ is the distance from r_0 to the surface in direction $\hat{\Omega}$, and $l_s(\Omega)$ is the chord length from a point on the surface across the region to the exit surface in the direction $\hat{\Omega}$. The solid angle subtended at r_0 by a differential surface area ds in the direction $\hat{\Omega}$ is

$$d\Omega = (\hat{\Omega} \cdot \hat{n}_s) ds / l^2(r_0, \Omega)$$

The average first flight escape probability for neutral particles created uniformly over the region is

$$P_0 = \frac{1}{V} \int P_0'(r_0) dV = \frac{1}{V} \int dV \int d\Omega \frac{e^{-l/(r_0, \Omega)/\lambda}}{4\pi} \quad (18)$$

If we take the volume of the region to be made up of tubular elements oriented in the $\hat{\Omega}$ direction, with cross-section area $ds(\hat{\Omega} \cdot \hat{n}_i)$, then $dV = (\hat{\Omega} \cdot \hat{n}_i) ds dl$ and Eq. (18) can be integrated over l to obtain

$$P_0 = \frac{\lambda}{4\pi V} \int\int ds d\Omega (\hat{\Omega} \cdot \hat{n}_i)(1 - e^{-l_s(\Omega)/\lambda}) \quad (19)$$

The concept of chord length (l_s) distribution is now introduced to reduce Eq. (19) to a form that can more readily be approximated. We define the probability that a chord is of length between l_s and $l_s + dl_s$

$$\phi(l_s) dl_s \equiv \frac{\int \left[\int_{l_s' = l_s} (\hat{\Omega} \cdot \hat{n}_i) d\Omega \right] ds}{\int\int (\hat{\Omega} \cdot \hat{n}_i) d\Omega ds}, \quad (\hat{\Omega} \cdot \hat{n}_i) > 0 \quad (20)$$

where the integral over Ω in the numerator is limited to those values of Ω for which $l_s'(\Omega) = l_s$. The denominator is readily evaluated

$$\int\int (\hat{\Omega} \cdot \hat{n}_i) d\Omega ds = 2\pi S \int_0^1 \mu d\mu = \pi S$$

where S is the surface area bounding the region.

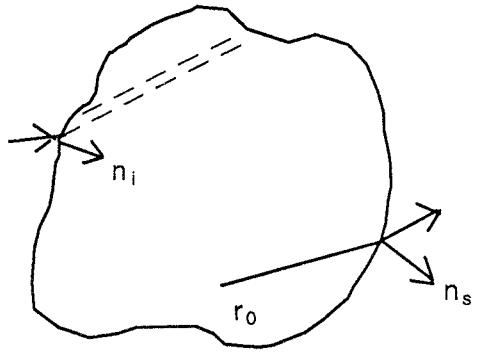

FIG. 4. Escape probability geometry.

The volume of the region is

$$V = \int l(\hat{\Omega}\cdot\hat{n}_i)\mathrm{d}s, \qquad (\hat{\Omega}\cdot\hat{n}_i) > 0$$

and the mean chord length is

$$\bar{l}_s \equiv \int l_s\phi(l_s)\mathrm{d}l_s = \frac{1}{\pi S}\int l_s\left[\int\int_{l'=l_s}(\hat{\Omega}\cdot\hat{n}_i)\mathrm{d}\Omega\mathrm{d}s\right]\mathrm{d}l_s$$

$$= \frac{1}{\pi S}\int\int l(\hat{\Omega}\cdot\hat{n}_i)\mathrm{d}\Omega\mathrm{d}s = \frac{4V}{S}, \qquad (\hat{\Omega}\cdot\hat{n}_i) > 0 \quad (21)$$

Hence,

$$\frac{4\pi V}{l_s}\phi(l)\mathrm{d}l = \int\left[\int_{e'}(\hat{\Omega}\cdot\hat{n}_i)\mathrm{d}\Omega\right]\mathrm{d}s(\hat{\Omega}\cdot\hat{n}_i) > 0 \qquad (22)$$

Using Eq. (22) in Eq. (19) leads to

$$P_0 = \frac{\lambda}{\bar{l}_s}\int (1 - \mathrm{e}^{l_s/\lambda})\phi(l_s)\mathrm{d}l_s$$

$$= \frac{\lambda}{\bar{l}_s} - \int \mathrm{e}^{-l_s/\lambda}\phi(l_s)\mathrm{d}l_s \qquad (23)$$

When the dimensions of the region are small compared to the mean free path, $l_s \ll \lambda$, Eq. (23) reduces to

$$P_0 \simeq 1 - \frac{1}{2}\frac{(\bar{l}_s^2)}{\bar{l}_s\lambda} \simeq 1 \qquad (24)$$

and when $l_s \gg \lambda$

$$P_0 \simeq \frac{\lambda}{\bar{l}_s} = \frac{\lambda S}{4V} \qquad (25)$$

This suggests the rational approximation

$$P_0 = \frac{1}{1 + \dfrac{4V}{\lambda S}} \qquad (26)$$

The particle may escape from the region uncollided, with probability P_0; its progeny may escape after one collision, with probability $(1 - P_0)A_{cx}P_0$; etc. The total escape probability for a neutral particle or its neutral progeny is

$$P = P_0 + (1 - P_0)P_0A_{cx} + (1 - P_0)^2(A_{cx})^2P_0 + \ldots$$

$$= P_0\sum_{n=0}^{\infty}(A_{cx}(1 - P_0))^n = \frac{P_0}{1 - A_{cx}(1 - P_0)} \qquad (27)$$

The distribution of escaping neutral particles among contiguous regions can be estimated from considerations of surface area (length in a 2-D model) and the motion of the progenitor ion in the case of a charge exchange neutral. An ion moves along a field line with its thermal speed; if there is a net ion flow, $\bar{v}_\parallel$, then

$$n\bar{v}_\parallel = \int_{-\infty}^{0} f(v_\parallel)v_\parallel\mathrm{d}v_\parallel + \int_0^{\infty} f(v_\parallel)v_\parallel\mathrm{d}v_\parallel$$

$$\equiv -n^-v_{th} + n^+v_{th} \qquad (28)$$

where n^+ and n^- are the number of ions moving parallel and antiparallel, respectively, to the field direction. Ion motion perpendicular to the field line has no preferential direction. Thus, the relative probability that a charge exchange neutral will escape from i into region j depends on the relative length (L_{ij}) of the interface between regions i and j and on the orientation of that interface with respect to the magnetic field

$$\Lambda_{i-j} = \text{const.}\, L_{ij}(|\hat{n}_\parallel \times \hat{n}_{ij}| + (\hat{n}_\parallel\cdot\hat{n}_{ij})\bar{v}_\parallel/v_{th}) \qquad (29)$$

where $\hat{n}_\parallel$ is the unit vector along the field line and $\hat{n}_{ij}$ is the normal unit vector to L_{ij} pointing from region i to region j. The constant is determined from the requirement

$$\sum_j^i \Lambda_{i-j} = 1$$

8. PLASMA ALBEDO

Neutrals crossing the separatrix from the SOL into the plasma edge region will either be ionized immediately or will undergo a sequence of charge exchange events terminating in ionization, with the result that a negligible number of neutrals penetrate beyond the plasma edge region. However, some of the charge exchange neutrals will re-emerge from the plasma edge back into the SOL.

Treating the plasma as an infinite half space for neutrals entering from the SOL and making use of the diffusion theory approximation, the plasma albedo is, by analogy to the neutron diffusion theory result [4],

$$\alpha_{\text{edge SOL}} \equiv \frac{\Gamma_{\text{edge SOL}}}{\Gamma_{\text{SOL edge}}} = \frac{1 - \dfrac{2}{\sqrt{3}}(A_{cx}^{-1} - 1)^{1/2}}{1 + \dfrac{2}{\sqrt{3}}(A_{cx}^{-1} - 1)^{1/2}} \qquad (30)$$

where A_{cx} is the charge exchange probability in the plasma edge region.

9. MODIFICATIONS TO TREAT A NEUTRAL IMPURITY SPECIES

The principal modification of the above formalism that is required in order to treat the transport of neutral impurity atoms is the replacement of the expression for the neutral flux from the wall into region i given by Eq. (3) with

$$\Gamma^{z}_{iw-i} = \sum_{a} \left((1 - f^{a}_{pi}) Y^{a-z}_{wi} \left\{ \sum_{k}^{i} \Gamma^{a}_{k-i} \left[T^{i,a}_{k-iw} + A^{i,a}_{cx} P^{a}_{i} \Lambda^{a}_{i-iw} \left(1 - \sum_{l}^{i} T^{i,a}_{k-l} \right) \right] + S^{i,a}_{ex} P^{a}_{i} \Lambda^{a}_{i-iw} \right\} \right) + \sum_{b} \Phi^{iw,b}_{plate} Y^{b-z}_{wi} \delta_{iw,ps} \quad (31)$$

The sums over a and b are over all neutral and ionic species, respectively. The quantities Y^{a-z}_{wi} and Y^{b-z}_{wi} are the sputtering yields of impurity neutrals of species z per neutral of species a or ion of species b, respectively, striking the wall of region i. Equation (25) can be generalized to have a different sputtering yield for each component of the neutral flux to the wall, evaluated for the energy corresponding to the region of origin of the neutral flux component. The other quantities have been defined previously without the species dependent superscripts a and b.

10. BENCHMARK AND MODEL PROBLEM CALCULATIONS

The transmission and escape probability model for neutral transport, as described in the previous sections, has been implemented in a computational code (GT-NEUT) and applied to two plasma edge neutral transport problems.

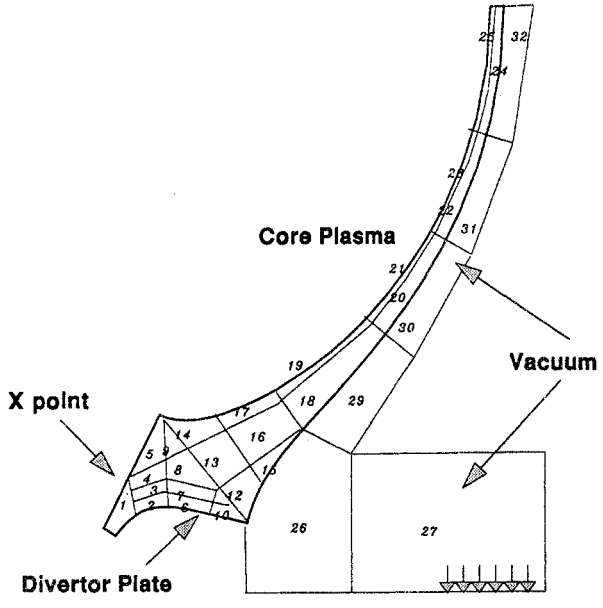

FIG. 5. Geometry of the benchmark problem with DEGAS 2. The numbered regions shown correspond to the GT-NEUT regions. The horizontal extent of the problem is 1.6 m, and the vertical extent is 2 m.

First, in order to establish the accuracy of the model, a benchmark calculation with the recently upgraded neutral transport Monte Carlo code DEGAS 2 [5, 6] was performed. The benchmark problem corresponds to the geometry shown in Fig. 5. The solution region contains the outboard SOL plasma, including part of the private flux area, a small part of the edge plasma (just inside the separatrix) and the associated vacuum regions. The calculation is carried out over a fixed plasma background with parameters covering a wide range of values: in the SOL region, the plasma density varies from 0.6×10^{20} m^{-3} in region 24 near the midplane to 1.14×10^{20} m^{-3} in region 2 near the divertor plate, while the electron temperature ranges from 170 eV in region 24 to 15 eV near the divertor plate. The DEGAS 2 run used 1152 (24×48) cells, while the GT-NEUT run had 25 SOL /divertor and 7 vacuum regions which are shown in Fig. 5. In both codes, charge exchange and ionization were the only atomic processes included. A unit source of neutral hydrogen atoms with energy $E_0 = 10$ eV was assumed and the source neutrals were launched uniformly into region 6 from the divertor plate. Since each GT-NEUT region contains a large number of DEGAS 2 cells, the plasma parameters were taken to be the corresponding volume averages (density weighted for the plasma temperatures) from the DEGAS 2 input data. The DEGAS 2 calculations required 7.5 min on the SPARC 10, and the GT-NEUT calculations required 5 s on the same machine.

The results from this comparison are shown in Fig. 6, where the total ionization rate per region is plotted for the two cases (the region number corresponds to Fig. 5). The DEGAS 2 rates are the sum of the total ionization rates in all DEGAS cells contained within each of the GT-NEUT regions. Regions 26–32 are vacuum regions which GT-NEUT treats as very low density and temperature plasma, resulting in a small but finite ionization rate. In DEGAS 2, vacuum regions are assigned zero ionization rate.

It can be seen that the agreement between the two codes is very good. The largest discrepancies occurred in the private flux region (1) and in the SOL regions towards the midplane (regions 18–25). Comparison with another DEGAS 2 case, where the neutrals were launched with a cosine velocity distribution, resulted in equally good agreement with the GT-NEUT code, indicating little sensitivity of the results to the isotropic incident flux model used in GT-NEUT. This is probably due to the strong charge exchange in front of the divertor plate, which diminishes the effect of the initial distribution of the launched neutrals [7].

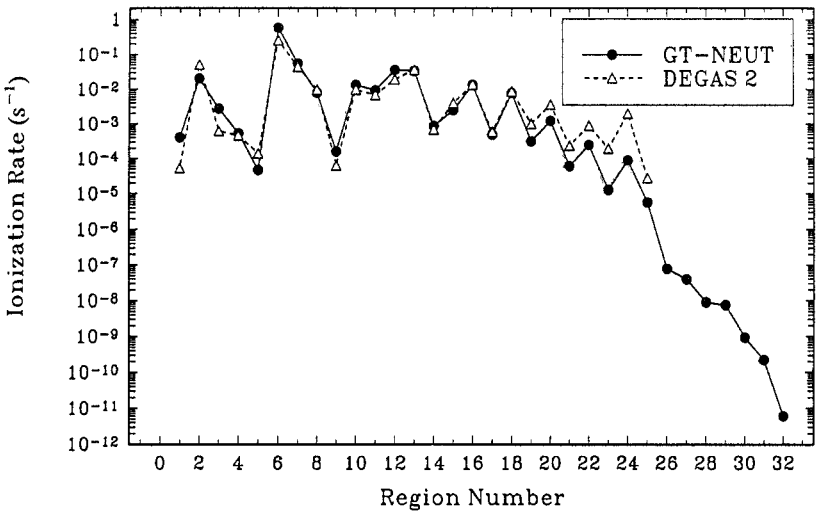

FIG. 6. Total ionization rate per region comparison between the transmission/escape probability neutral transport code GT-NEUT and the DEGAS 2 Monte Carlo code.

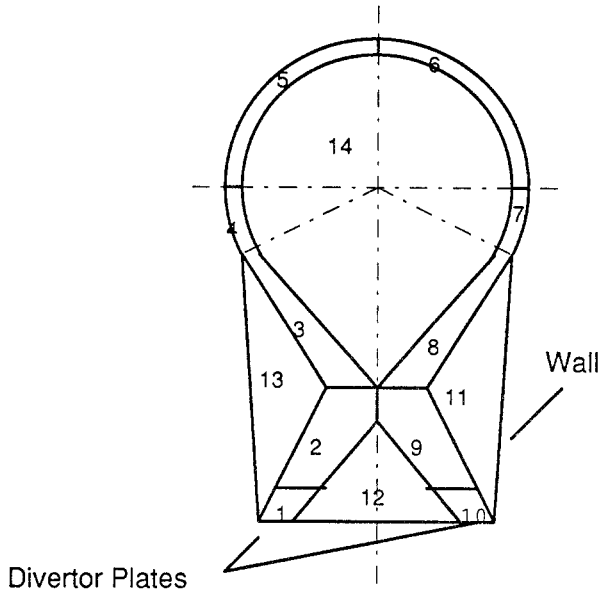

FIG. 7. Geometry for the ITER model problem.

The GT-NEUT calculations also illustrate the importance of including the vacuum regions when calculating the transport of neutrals at the plasma edge. Running the same problem but without the vacuum regions 26–32, the resulting ionization rate was found to be orders of magnitude smaller in the upper part of the SOL plasma (regions 18–25) compared to the DEGAS 2 prediction and to the GT-NEUT solution with the vacuum regions included. Without these vacuum regions, neutrals near the divertor regions cannot free-stream up towards the midplane. This ability to treat transport in complex geometries and across low and high mean free path regions is one of the most attractive features of the transmission/escape probabilities method, compared to other approximate methods of neutral transport, which generally lack this capability.

We have not compared the transmission/escape probabilities method with methods based on the diffusion theory approximation, since diffusion theory would not be appropriate for the complicated geometry and vacuum regions of the benchmark problem. However, comparisons between DEGAS and neutral diffusion theory calculations in an idealized geometry have been published recently [8].

Next, the method was applied to analyse the transport of neutrals in the edge of a plasma characteristic of a single-null ITER configuration. The (simplified) geometry of our model problem is shown in Fig. 7. The background plasma densities and temperatures vary from 1.2×10^{20} m^{-3} and 25 eV in region 1 in front of the divertor plate to 0.2×10^{20} m^{-3} and 230 eV at the symmetry point on top of the SOL region. Hydrogen neutrals of 100 eV energy were assumed for the evaluation of mean free paths. The total ion flux incident upon the two divertor plates in regions 1 and 10 was taken to be equal to 2.2×10^{22} s^{-1}, consistent with reference ITER particle confinement assumptions. This ion flux is reflected from the divertor plates as a neutral flux into regions 1 and 10 (see Eq. (7)).

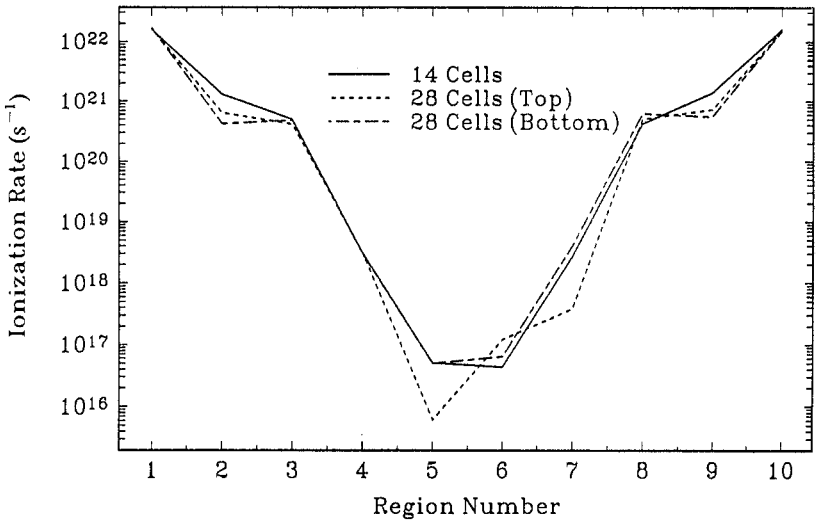

FIG. 8. Ionization rate for the ITER model problem, for three different divisions of the geometry.

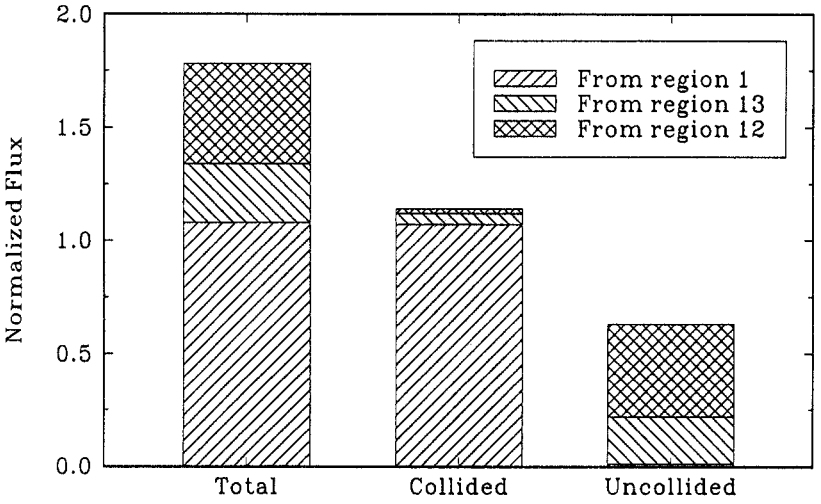

FIG. 9. Normalized flux distribution entering region 2. Only the contributions from regions 12, 13 and 1 are shown since those from adjacent regions 3 and 9 are negligible.

We first examined the sensitivity to the number of regions used to represent the SOL and divertor. The same problem was run with 14 regions and then with twice that number of regions, by subdividing further some of the 14 regions in the original case shown in Fig. 7. Two different divisions were performed, one emphasizing the top part of the SOL region (regions 3–8), and the other emphasizing the region near the divertor (regions 1–2, 9–10).

The results of the simulations are shown in Fig. 8, where the total ionization rate is plotted for each region of Fig. 7. It can be seen that the results are not very sensitive to the number of regions used to represent the SOL and divertor, particularly in areas of high ionization rates.

To illustrate the relative magnitudes of the different fluxes that enter the calculation, the total, collided and uncollided fluxes (Eq. (1)) for the problem of Fig. 7 are plotted for region 2 in Fig. 9. It can be seen that most of the flux to region 2 originates from region 1, which is bounded by the inboard divertor plate. Most of this flux emerges from region 1 as collided flux, since the electron

density in region 1 is rather high. The uncollided flux entering region 2, about 30% of the total flux, comes mostly from the two adjacent vacuum regions 12 and 13, where the ionization mean free paths are very long.

11. DISCUSSION

The appeal of the proposed model is its ability to accurately and economically calculate neutral transport in a complex 2-D geometry with regions of widely varying mean free path. The geometrical complexity enters via transmission and escape probabilities which can be precomputed as a function of the mean free path and obtained from tables at run time. The geometrical models of Fig. 2 or Fig. 7 serve to quantify the number of equations that might be involved in a typical application. There are 2 flux equations for each 'internal' surface and 1 flux equation for each 'external' surface bounded by either the plasma or the wall, for a total of 64 equations in the case of Fig. 2. The coupling among surface fluxes is nearest-neighbour, so the matrix **M** of Eq. (7) is relatively sparse.

While the geometrical models of Figs 2 and 7 are composed of regions that are bounded by straight lines and arcs of circles, and the transmission probabilities given in the appendices are for such a geometry, this is not a limitation on the model. Once the geometry is specified, no matter how complex, the transmission and escape probabilities can be precomputed numerically and only a table lookup is needed at run time.

The transmission probabilities are exact, subject to three assumptions: (1) uniform mean free path; (2) isotropic angular distribution of the incident flux over the inward hemisphere; and (3) uniform distribution of the incident flux over the surface. All of these assumptions can be removed by generalizing to known flux variations. The first assumption is not so limiting as it appears to be, since the transmission calculated with an exponentially varying density between two surfaces is the same as that which would be calculated using the average density. The second assumption should be valid except near corners joining regions of very different mean free paths. The consequences of the third assumption could be ameliorated by subdividing surfaces, if necessary.

The first-flight escape probabilities are exact, subject to three assumptions: (1) uniform mean free path; (2) isotropic angular distribution of 'secondary' charge exchange and external source neutrals; and (3) uniform spatial distribution of charge exchange and external source neutrals. Again, the first assumption is not as limiting as it seems. The second assumption is quite plausible. The third assumption is perhaps questionable for virgin source neutrals and first-collision charge exchange neutrals in some regions, but is quite plausible for those neutrals escaping after two or more charge exchange events. It should be noted, however, that the simple expression $P_0 \simeq S\lambda/4V$ is subject to the further assumption that the region is large compared to a mean free path.

The methodology proposed in this paper lends itself to taking into account differences in the speeds of neutrals that originate in different regions and thus using the correct mean free paths in determining transmission and attenuation. This is an intrinsic advantage of an integral transport based method over a differential transport based method, which would require an additional modelling of energy transfer (e.g. a multigroup model). However, a multigroup method can be used with the transmission /escape probabilities method.

It is felt that the methodology proposed in this paper can lead both to relatively simple neutral transport models that can be used with simple '2-point' plasma models of the SOL and divertor for scoping and parameter studies and to detailed neutral transport models that can be used with 1-D and 2-D plasma models of the SOL and divertor for detailed analysis of experiment and divertor design. Such models should be able to produce greater accuracy for a given computational time than other models presently available for the calculation of neutral transport in the outer regions of a diverted tokamak. The benchmark comparisons with DEGAS 2 and the ITER model calculations reported in Section 10 support these contentions.

Appendix A

DISCUSSION OF NEUTRAL PARTICLE COMPUTATIONAL METHODS

There are three general categories of neutral computational models, based on: (1) approximation to the integral form of the transport equation; (2) approximation to the differential form of the transport equation; or (3) simulation of particle transport by following a large number of randomly generated particle histories and statistically averaging the results (Monte Carlo).

The integral transport equation [3] states that, for a given source of particles, those particles going in a given direction are exponentially attenuated as the integral of the inverse mean free path along the direction of flight. For a fixed solution is a straightforward matter of geometry. However, when one of the processes that

attenuates the neutrals results in other neutrals with different energy and direction, this process constitutes a secondary neutral source which is distributed in space, and so on for tertiary, quartiary, etc. neutral sources. Charge exchange is one such process for neutrals in the outer regions of a plasma. Thus, the solution of the integral transport equation must proceed iteratively, with an approximate evaluation of the distributed source and an exact solution of the particle transport from the approximate source constituting the iteration step. Because of the coupling among all spatial points that is inherent to the integral transport formulation, this iterative solution can become very computationally intensive for any but the simplest situations. In practice (see for example, Ref. [9]) the integral transport solution is obtained for the attenuation of particles coming from a fixed source, such as reflection from the wall, and secondary distributed sources are neglected. Such a treatment is satisfactory when the ionization rate is much greater than the charge exchange rate, but is poor when the two rates are comparable, which is the case in many parts of the outer regions of a plasma.

Approximations based on the differential formulation of the transport equation have been highly developed for neutron transport in connection with nuclear reactor calculations, where they proved to be more practically useful than approximations based on the integral formulation, in general. Two general classes of approximation were developed, distinguished by the treatment of the angular dependence. In the spherical harmonics, or P_n, method (see, for example, Ref. [2]), the angular dependence of the neutral distribution is expanded in spherical harmonics, and moments equations are generated by integrating over angle and making use of orthogonality relations. In principle, any degree of angular anisotropy can be treated by taking enough moments. In practice, these methods found their greatest application in one dimensional problems where a few Legendre polynomials sufficed to represent the angular distribution. In the discrete ordinates, or S_n, method (see, for example, Ref. [10]), the transport equation is only solved at a few angular directions (ordinates), with the integrals over angle that enter these equations being approximated by a quadrature involving values at these ordinates and a quadrature weight, the choice of which is quite important. When the angular distribution can be represented by a linearly anisotropic spherical harmonics approximation or by a two-ordinate discrete ordinates approximation, the lowest order approximation that results is diffusion theory (see, for example, Ref. [11]). These approximations to the differential transport equation also must be solved iteratively but, because the coupling among spatial points is nearest-neighbour, the iterative procedure is more tractable than for the integral formulation. The diffusion approximation is widely used in neutron transport for 1-D, 2-D and 3-D calculations in which the linear anisotropy assumption is valid, and higher order discrete ordinates approximations are the method commonly employed in 1-D and 2-D problems when higher order anisotropy in the angular distribution must be included.

Discrete ordinates codes that had been developed for neutron transport were applied to calculate neutral transport in the edge of simple plasma models represented by slab or cylindrical geometry several years ago (see, for example Refs [12–14]), but this method does not seem to have been applied recently or extended to the more complex geometry of the outer regions of a diverted tokamak plasma. The diffusion approximation has been applied to plasma outer region calculations recently (see, for example, Ref. [15]), but the diffusion theory assumption of linear anisotropy in the angular distribution would seem to be invalid in many cases of interest (e.g. the reflection of ions from a wall as neutrals, the interface between a divertor channel in which there is ionization and charge exchange and a plenum region in which there is free streaming). We are not aware of an application of P_n or double P_n methods. Double P_1 methods, in which the angular distribution is assumed isotropic within each of two hemispheres, would seem to offer significant advances in accuracy over diffusion theory in 1-D situations. Because of the inherent 2-D geometry and angular anisotropy, the discrete ordinates methods would seem to be the best suited of the approximations based on the differential transport formulation for application to neutral transport in the plasma outer regions.

Monte Carlo calculations simulate the fates of many randomly generated particles to obtain an averaged solution for the transport of a population of neutral particles. This methodology (see, for example, Ref. [16]) is highly developed, and, because of previous emphasis upon applications to complex geometries, has good capability to represent the geometrical complexity of the plasma and divertor chambers. Monte Carlo has been extensively applied to the computation of neutral particle transport in the outer regions of diverted tokamaks (see, for example, Refs [5, 17]). Extreme high accuracy can be obtained with Monte Carlo, provided that the basic reaction rate parameters are well known and that a sufficient number of histories are simulated for the statistical uncertainty in the averaged solution to be acceptably small. This latter condition can lead to particularly demanding computational requirements when the Monte Carlo solution is part of a neutral–charged particle iterative solution procedure, since convergence of the outer neutral–charged particle

iteration can be destroyed by statistical fluctuations in the Monte Carlo solutions on successive iterates. Monte Carlo will probably remain as the ultimate method for neutral particle transport in diverted tokamak plasmas in cases where high accuracy in a complex geometry is required and computational time is a secondary consideration. However, for routine calculations, the discrete ordinates method and the method presented in this paper would seem to have certain computational advantages.

Appendix B

TRANSMISSION PROBABILITIES FOR STRAIGHTLINE GEOMETRIES

For a region bounded by straight line segments, two situations can be distinguished: (1) transmission between adjacent, intersecting sides; and (2) transmission between non-adjacent, non-intersecting sides. The transmission probabilities are calculated under the assumption that the incident flux is isotropic over the incident hemisphere and uniform over the incident surface.

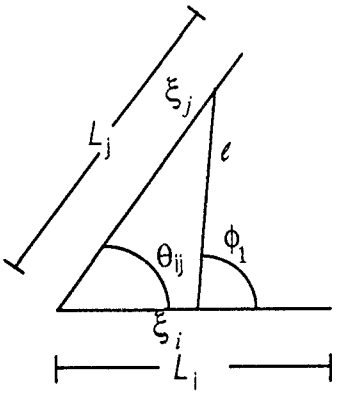

FIG. 10. Adjacent side.

B.1. Adjacent, intersecting sides with included angle θ_{ij} (Fig. 10)

The local transmission probability for a point (ξ_i) on side i to side j, as defined by Eq. (15), is given by

$$t_{i-j}(\xi_i) = \frac{1}{\pi}\int_0^{L_j} d\xi_j \left|\frac{d\phi_1}{d\xi_j}\right| e^{-\xi_j \sin\theta_{ij}/\lambda \sin\phi_1} \tag{32}$$

where

$$\phi_1(\xi_i, \xi_j) = \cot^{-1}\left(\cot\theta_{ij} - \frac{\xi_i}{\xi_j \sin\theta_{ij}}\right) \tag{33}$$

and

$$\left|\frac{d\phi_1}{d\xi_j}\right| = \frac{\xi_i/\xi_j^2 \sin\theta_{ij}}{1 + \left(\cot\theta_{ij} - \frac{\xi_i}{\xi_j \sin\theta_{ij}}\right)^2} \tag{34}$$

where (ξ_i) is the distance along side i measured from the intersection.

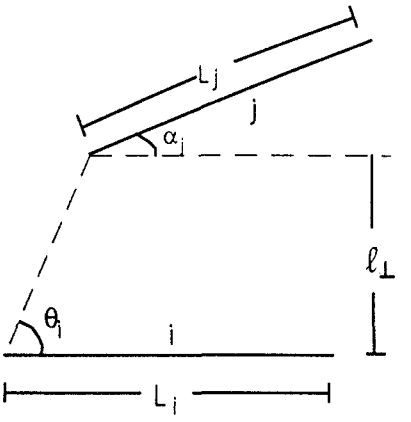

FIG. 11. Non-adjacent sides.

B.2. Non-adjacent, non-intersecting sides (Fig. 11)

The local transmission probability, given by Eq. (15), from a point (ξ_i) on side i to side j is given by

$$t_{i-j}(\xi_i) = \frac{1}{\pi}\int_0^{L_j} d\xi_j \left|\frac{d\phi_2}{d\xi_j}\right| e^{-(l_\perp + \xi_j \sin\alpha_j)/\lambda \sin\phi_2} \tag{35}$$

where

$$\left|\frac{d\phi_2}{d\xi_j}\right| = \frac{1}{1 + \left(\frac{l_\perp \cot\theta_i + \xi_j \cos\alpha_j - \xi_i}{l_\perp + \xi_j \sin\alpha_j}\right)^2} \times \frac{\xi_i \sin\alpha_j + l_\perp(\cos\alpha_j - \sin\alpha_j \cot\theta_i)}{(l_\perp + \xi_j \sin\alpha_j)^2} \tag{36}$$

and

$$\phi_2(\xi_i, \xi_j) = \cot^{-1}\left(\frac{\xi_j \cos\alpha_j - \xi_i + l_\perp \cot\theta_i}{l_\perp + \xi_j \sin\alpha_j}\right) \tag{37}$$

and ξ_j is measured along side j from left to right.

The total transmission probability of Eq. (16) is given by

$$T_{i-j} = \int_0^{L_i} d\xi_i t_{i-j}(\xi_i)/L_i \tag{38}$$

for both cases.

Appendix C

TRANSMISSION PROBABILITIES FOR ANNULAR SEGMENTS

The geometry of an annular segment can be characterized by the angle ($\Delta\theta$) subtended by the segment and by the inner (R_{in}) and outer (R_{out}) radii of the segment. The calculation of transmission probabilities must take into account the facts that some points on each surface cannot be 'seen' by a straight line of sight from some points on another surface and that there is transmission from an inwardly concave outer surface to itself. The transmission probabilities are calculated under the assumptions that the angular distribution of the incident flux is isotropic over the inward hemisphere and that the spatial distribution of the incident flux is uniform over the surface. Figure 12 illustrates the annular segment geometry.

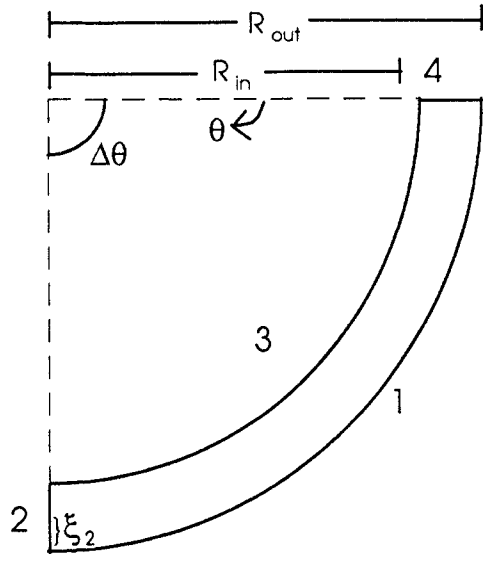

FIG. 12. Annular segment geometry.

C.1. Transmission from an outer, concave-inward surface (i.e. side 1)

The local self-transmission probability, defined by Eq. (12), for a point (R_{out}, θ) on the outer surface 1 to surface 1 is given by

$$t_{1\text{-}1}(\theta) = \frac{1}{\pi}\int_{\theta^{11}_{min}(\theta)}^{\theta^{11}_{max}(\theta)} d\theta' \left|\frac{d\phi^{11}}{d\theta'}\right| e^{-2R_{out}\sin\left(\frac{|\theta-\theta'|}{2}\right)/\lambda} \tag{39}$$

where

$$\left|\frac{d\phi^{11}}{d\theta'}\right| = \frac{1}{2}$$

and

$$\theta^{11}_{min}(\theta) = \max\left\{0, \theta - 2\cos^{-1}\left(\frac{R_{in}}{R_{out}}\right)\right\}$$

$$\theta^{11}_{max}(\theta) = \min\left\{\Delta\theta, \theta + 2\cos^{-1}\left(\frac{R_{in}}{R_{out}}\right)\right\} \tag{40}$$

The local transmission probability from a point (R_{out}, θ) on the outer surface 1 to the radial surface 4 is given by

$$t_{1\text{-}4}(\theta) = \frac{1}{\pi}\int_{\phi^{14}_{min}(\theta)}^{\phi^{14}_{max}(\theta)} d\phi e^{-R_{out}\sin\theta/\lambda\sin(\phi+\theta)} \tag{41}$$

where

$$\phi^{14}_{min}(\theta) = \max\left\{\left(\frac{\pi}{2} - \cos^{-1}\frac{R_{in}}{R_{out}}\right), \cot^{-1}\left(\frac{R_{out}}{R_{in}}\frac{1}{\sin\theta} - \cot\theta\right)\right\}$$

$$\phi^{14}_{max}(\theta) = \max\left\{\phi^{14}_{min}(\theta), \left(\frac{\pi}{2} - \frac{\theta}{2}\right)\right\} \tag{42}$$

The local transmission probability to the other radial surface 2 is obtained from Eqs (41) and (42) by replacing $\theta \rightarrow \Delta\theta - \theta$ and $4 \rightarrow 2$.

The local transmission probability from a point (R_{out}, θ) on the outer surface 1 to the inner surface 3 is given by

$$t_{1\text{-}3}(\theta) = \frac{1}{\pi}\int_{\theta^{13}_{min}(\theta)}^{\theta^{13}_{max}(\theta)} d\theta' \left|\frac{d\phi^{13}}{d\theta'}\right| e^{-R_{in}\sin(|\theta-\theta'|)/\lambda\sin\phi^{13}(\theta,\theta')} \tag{43}$$

where

$$\phi^{13}(\theta,\theta') = \cot^{-1}\left[\frac{R_{out}}{R_{in}\sin(|\theta-\theta'|)} - \cot(|\theta-\theta'|)\right] \tag{44}$$

$$\frac{d}{d\theta'}\phi^{13}(\theta,\theta') = -\frac{\sigma\left\{\dfrac{-R_{out}\cos(\theta-\theta') + R_{in}}{R_{in}\sin^2(\theta-\theta')}\right\}}{1 + \left\{\dfrac{R_{out}}{R_{in}\sin(|\theta-\theta'|)} - \cot(|\theta-\theta'|)\right\}^2} \tag{45}$$

with

$$\sigma \equiv \frac{\theta' - \theta}{|\theta' - \theta|}$$

and

$$\theta^{13}_{\min}(\theta) = \max\left\{0, \theta - \cos^{-1}\left(\frac{R_{in}}{R_{out}}\right)\right\} \quad (46a)$$

$$\theta^{13}_{\max}(\theta) = \min\left\{\Delta\theta, \theta + \cos^{-1}\left(\frac{R_{in}}{R_{out}}\right)\right\} \quad (46b)$$

The total transmission probabilities, given by Eq. (16), for transmission from the outer surface to surface j are evaluated from

$$T_{1-j} = \frac{1}{\Delta\theta}\int_0^{\Delta\theta} d\theta\, t_{1-j}(\theta) \quad (47)$$

C.2. Transmission from an inner, convex-inward surface (i.e. side 3)

The local transmission probability from a point (R_{in}, θ) on the inner surface 3 to the radial surface 4 is given by

$$t_{3-4}(\theta) = \frac{1}{\pi}\int_{\phi^{34}_{\min}(\theta)}^{\phi^{34}_{\max}(\theta)} d\phi e^{-R_{in}\sin\theta/\lambda\sin(\phi+\theta)} \quad (48)$$

where

$$\phi^{34}_{\min}(\theta) = \frac{\pi}{2} \quad (49a)$$

$$\phi^{34}_{\max}(\theta) = \max\left\{\frac{\pi}{2}, \cot^{-1}\left[\frac{R_{in}}{R_{out}\sin\theta} - \cot\theta\right]\right\} \quad (49b)$$

It can be seen that if

$$\theta \geq \theta^* \equiv \cos^{-1}\left(\frac{R_{in}}{R_{out}}\right)$$

then $t_{3-4}(\theta) = 0$.

The local transmission probability from a point on the inner surface to the other radial surface 2 is given by Eqs (48) and (49) with the replacements $\theta \rightarrow \Delta\theta - \theta$ and $4 \rightarrow 2$.

The local transmission probability from a point (R_{in}, θ) on the inner surface 3 to the outer surface 1 is given by

$$t_{3-1}(\theta) = \frac{1}{\pi}\int_{\theta^{31}_{\min}(\theta)}^{\theta^{31}_{\max}(\theta)} d\theta \left|\frac{d\phi^{31}}{d\theta'}\right| e^{-R_{out}\sin(|\theta-\theta'|)/\lambda\cos\phi^{31}(\theta,\theta')} \quad (50)$$

where

$$\phi^{31}(\theta,\theta') = \tan^{-1}\left(\cot(|\theta-\theta'|) - \frac{1}{\sin(|\theta-\theta'|)}\frac{R_{in}}{R_{out}}\right) \quad (51)$$

and

$$\frac{d\phi^{31}}{d\theta'} = \frac{\sigma\left(\frac{R_{in}\cos(\theta-\theta') - R_{out}}{R_{out}\sin^2(\theta-\theta')}\right)}{1 + \left(\cot(|\theta-\theta'|) - \frac{1}{\sin(|\theta-\theta'|)}\frac{R_{in}}{R_{out}}\right)^2}$$

where

$$\sigma = \frac{\theta' - \theta}{|\theta' - \theta|} \quad (52)$$

$$\theta^{31}_{\min}(\theta) = \max\left\{0, \theta - \cos^{-1}\left(\frac{R_{in}}{R_{out}}\right)\right\} \quad (53a)$$

$$\theta^{31}_{\max}(\theta) = \min\left\{\Delta\theta, \theta + \cos^{-1}\left(\frac{R_{in}}{R_{out}}\right)\right\} \quad (53b)$$

The total transmission probability for transmission from the inner surface 3 to surface j is given by

$$T_{3-j} = \frac{1}{\Delta\theta}\int_0^{\Delta\theta} d\theta\, t_{3-j}(\theta) \quad (54)$$

C.3. Transmission from a radial surface (e.g. side 2)

The local transmission probability for a point $(R_{out} - \xi, \Delta\theta)$ on the radial surface 2 to the inner surface 3 is given by

$$t_{2-3}(\xi_2) = \frac{1}{\pi}\int_{\theta^{23}_{\min}(\xi_2)}^{\Delta\theta} d\theta \left|\frac{d\phi^{23}}{d\theta}\right| e^{-R_{in}\sin(\Delta\theta-\theta)/\lambda\sin\phi^{23}} \quad (55)$$

where

$$\phi^{23}(\xi_2,\theta) = \cot^{-1}\left(\frac{R_{out} - \xi_2}{R_{in}\sin(\Delta\theta - \theta)} - \cot(\Delta\theta - \theta)\right) \quad (56)$$

and

$$\frac{d\phi^{23}}{d\theta} = -\frac{\frac{(R_{out} - \xi_2)\cos(\Delta\theta - \theta) - R_{in}}{R_{in}\sin^2(\Delta\theta - \theta)}}{1 + \left(\frac{R_{out} - \xi_2}{R_{in}\sin(\Delta\theta - \theta)} - \cot(\Delta\theta - \theta)\right)^2} \quad (57)$$

$$\theta^{23}_{\min}(\xi_2) = \max\left\{0, \Delta\theta - \cos^{-1}\left(\frac{R_{in}}{R_{out} - \xi_2}\right)\right\} \quad (58)$$

The local transmission probability for a point $(R_{out} - \xi_2, \Delta\theta)$ on the radial surface 2 to the outer surface 1 is given by

$$t_{2-1}(\xi_2) = \frac{1}{\pi}\int_{\theta^{21}_{\min}(\xi_2)}^{\Delta\theta} d\theta \left|\frac{d\phi^{21}}{d\theta}\right| e^{-R_{out}\sin(\Delta\theta-\theta)/\lambda\sin\phi^{21}} \quad (59)$$

where

$$\phi^{21}(\xi_2, \theta) = \cot^{-1}\left(\frac{R_{out} - \xi_2}{R_{out}\sin(\Delta\theta - \theta)} - \cot(\Delta\theta - \theta)\right) \quad (60)$$

and

$$\theta^{21}_{min}(\xi_2) = \max\left\{0, \Delta\theta - \cos^{-1}\frac{R_{in}}{R_{out} - \xi_2} - \cos^{-1}\frac{R_{in}}{R_{out}}\right\} \quad (61)$$

and

$$\frac{d\phi^{21}}{d\theta} = -\frac{\dfrac{(R_{out} - \xi_2)\cos(\Delta\theta - \theta) - R_{out}}{R_{out}\sin^2(\Delta\theta - \theta)}}{1 + \left(\dfrac{R_{out} - \xi_2}{R_{out}\sin(\Delta\theta - \theta)} - \cot(\Delta\theta - \theta)\right)^2} \quad (62)$$

The local transmission probability from a point $(R_{out} - \xi_2, \Delta\theta)$ on the radial surface 2 to the opposite radial surface 4 is given by

$$t_{2\text{-}4}(\xi_2) = \frac{1}{\pi}\int_0^{\xi_4^{max}(\xi_2)} d\xi_4 \left|\frac{d\phi^{24}}{d\xi_4}\right| e^{-(R_{out} - \xi_4)\sin\Delta\theta/\lambda\sin\phi^{24}} \quad (63)$$

where

$$\phi^{24}(\xi_2, \xi_4) = \cot^{-1}\left(\frac{R_{out} - \xi_2}{(R_{out} - \xi_4)\sin\Delta\theta} - \cot\Delta\theta\right) \quad (64)$$

and

$$\frac{d\phi^{24}}{d\xi_4} = -\frac{1}{1 + \left(\dfrac{R_{out} - \xi_2}{(R_{out} - \xi_4)\sin\Delta\theta} - \cot\Delta\theta\right)^2} \times \frac{R_{out} - \xi_2}{(R_{out} - \xi_4)^2\sin\Delta\theta} \quad (65)$$

$$\xi_4^{max}(\xi_2) = \min\left\{(R_{out} - R_{in}), R_{out} - \frac{R_{in}}{\sin(\phi^{24}_{tan} + \Delta\theta)}\right\} \quad (66)$$

where

$$\phi^{24}_{tan}(\xi_2) = \tan^{-1}\left(\frac{R_{in}}{\sqrt{(R_{out} - \xi_2)^2 - R_{in}^2}}\right) \quad (67)$$

If $\theta^* \equiv \cos^{-1}(R_{in}/R_{out}) \geq \Delta\theta/2$, then the radial surface 2 does not 'see' radial surface 4, and the transmission probability $t_{2\text{-}4}$ is identically equal to zero.

The local transmission probability for a point $(R_{out} - \xi_4, \theta = 0)$ on the radial surface 4 to the opposite radial surface 2 is given by Eqs (64)-(68) with the replacement $\Delta\theta - \theta \to \theta$ and the interchange of the subscripts 2 and 4 on ξ.

The various total transmission coefficients are given by

$$T_{2\text{-}j} = \frac{1}{R_{out} - R_{in}}\int_0^{R_{out} - R_{in}} d\xi_2\, t_{2\text{-}j}(\xi_2) \quad (68)$$

ACKNOWLEDGEMENTS

The authors would like to thank C.F.F. Karney for his help in setting up the benchmark problem with DEGAS 2 and for useful discussions. The help of R. Rubilar in the preparation of the input for the GT-NEUT code is also appreciated.

REFERENCES

[1] TENDLER, M., HEIFETZ, D., Fusion Technol. **11** (1987) 289.
[2] GELBARD, E.M., "Spherical harmonics methods: P_L and double-P_L approximations", Computing Methods in Reactor Physics (GREENSPAN, H., KELBER, C.N., OKRENT, D., Eds), Gordon and Breach, New York (1968) 271-364.
[3] CASE, K.M., et al., Introduction to the Theory of Neutron Diffusion, Vol. 1, Report, Los Alamos Scientific Lab., CA (1953).
[4] MEGHREBLIAN, R.V., HOLMES, D.K., Reactor Analysis, McGraw-Hill, New York (1960) 193-195.
[5] HEIFETZ, D., et al., J. Comput. Phys. **46** (1982) 309.
[6] KARNEY, C.F.F., STOTLER, D.P., Bull. Am. Phys. Soc. **38** (1993) 1919.
[7] KARNEY, C.F.F., Princeton Plasma Physics Lab., NJ, personal communication, 1994.
[8] VOLD, E.L., et al., Fusion Technol. **22** (1992) 208.
[9] BRAAMS, B.J., in Controlled Fusion and Plasma Physics (Proc. 11th Eur. Conf. Aachen, 1983), Vol. 7D, Part II, European Physical Society, Geneva (1984) 431; ibid., Vol. 9F, Part II, p. 480.
[10] CARLSON, B.G., LATHROP, K.D., Transport Theory: The Method of Discrete Ordinates, ibid., pp. 171-270.
[11] HASSITT, A., Diffusion Theory in Two and Three Dimensions, ibid., pp. 91-170.
[12] GREENSPAN, E., Nucl. Fusion **14** (1974) 771.
[13] MARABLE, J.H., OBLOW, E.M., Nucl. Sci. Eng. **61** (1976) 90.
[14] GILLIGAN, J.G., et al., Nucl. Fusion **18** (1978) 63.
[15] VOLD, E.L., et al., J. Nucl. Mater. **176-177** (1990) 570.
[16] KALOS, M.H., et al., "Monte Carlo methods in reactor computations", Computing Methods in Reactor Physics (GREENSPAN, H., KELBER, C.N., OKRENT, D., Eds), Gordon and Breach, New York (1968) 365-443.
[17] CUPINI, E., et al., NIMBUS-Monte Carlo Simulation of Neutral Particle Transport in Fusion Devices, NET Rep. EVR X11-324/9, NET Group, IPP, Garching (1984).

(Manuscript received 28 December 1992
Final manuscript received 22 April 1994)